macromol

MDPI

Communication

Influence of Thermal and Chemical Stresses on Thermal Properties, Crystal Morphology, and Mechanical Strength Development of a Sulfur Polymer Composite

Perla Y. Sauceda-Oloño, Claudia V. Lopez, Bhakti K. Patel, Ashlyn D. Smith * and Rhett C. Smith *

Department of Chemistry and Center for Optical Materials Science and Engineering Technology, Clemson University, Clemson, SC 29634, USA; psauced@g.clemson.edu (P.Y.S.-O.); cvlopez@g.clemson.edu (C.V.L.); bkpatel@g.clemson.edu (B.K.P.)

* Correspondence: ashlynd@clemson.edu (A.D.S.); rhett@clemson.edu (R.C.S.)

Abstract: The unique properties and sustainability advantages of sulfur polymer cement have led to efforts to use them as alternatives to traditional Portland cement. The current study explores the impact of environmental stresses on the strength development of polymer composite $SunBG_{90}$, a material composed of animal and plant fats/oils vulcanized with 90 wt. % sulfur. The environmental stresses investigated include low temperature (−25 °C), high temperature (40 °C), and submersion in water, hexanes, or aqueous solutions containing strong electrolyte, strong acid, or strong base. Samples were analyzed for the extent to which exposure to these stresses influenced the thermo-morphological properties and the compressional strength of the materials compared to identical materials allowed to develop strength at room temperature. Differential scanning calorimetry (DSC) analysis revealed distinct thermos-morphological transitions in stressed samples and the notable formation of metastable γ-sulfur in hexane-exposed specimens. Powder X-ray diffraction confirmed that the crystalline domains identified by DSC were primarily γ-sulfur, with ~5% contribution of γ-sulfur in hexane-exposed samples. Compressive strength testing revealed high strength retention other than aging at elevated temperatures, which led to ~50% loss of strength. These findings reveal influences on the strength development of $SunBG_{90}$, lending important insight into possible use as an alternative to OPC.

Keywords: sulfur; sustainable composites; polymer cements; compressive strength

Citation: Sauceda-Oloño, P.Y.; Lopez, C.V.; Patel, B.K.; Smith, A.D.; Smith, R.C. Influence of Thermal and Chemical Stresses on Thermal Properties, Crystal Morphology, and Mechanical Strength Development of a Sulfur Polymer Composite. *Macromol* **2024**, *4*, 240–252. https://doi.org/10.3390/macromol4020013

Academic Editor: Ana María Díez-Pascual

Received: 9 February 2024
Revised: 24 March 2024
Accepted: 16 April 2024
Published: 25 April 2024

1. Introduction

Sulfur polymer cements represent an alternative to ordinary Portland cement (OPC) with distinct advantages in terms of their mechanical and environmental durability properties [1–4]. The chemical composition of materials referred to as sulfur polymer cement in the literature varies greatly. At one extreme are formulations wherein elemental sulfur is used as a minority component or surface treatment of OPC, affording materials with increased resistance to low-pH environments. Other formulations employ a high sulfur content material (HSM) comprising 50–95 wt. % elemental sulfur without any added OPC as the cementitious binder itself. The properties of such polymer cement can be tuned by traditional concepts used to tune organic polymer properties. As a result, HSMs range from flexible high-tensile strain materials to rigid materials with higher compressive strength than ordinary Portland cement (OPC). Whereas OPC productions account for ~8% of anthropogenic CO_2—more than all non-commercial automobile emissions [5]—HSMs can be made by reacting fossil fuel waste sulfur with organic waste materials or bio-derived olefins. Each carbon atom in such HSMs represents a molecule of CO_2 removed from the atmosphere, so using HSMs in place of OPC could reduce humanity's carbon footprint and contribute to ecological preservation. Recent work has unveiled a range of potential

alternatives to OPC, including geopolymers [6,7] and sulfur cement/concrete [1,8–13] or HSMs. HSMs also prove applicable in a wider range of applications [14–33].

Compared to OPC, HSMs also offer advantages of setting and hardening times. HSMs demonstrate rapid setting and higher early strength gains. This desirable early-stage performance characteristic makes HSMs optimal materials for applications requiring fast turnaround times (hours to a few days versus over 28 days for many OCP formulations). The shorter window for full property development in HSMs also allows testing environmental influences on their mechanical strength development to be conducted more expeditiously. The HSM SunBG$_{90}$ (a composite made from 5 wt. % sunflower oil, 5 wt. % brown grease [34,35], and 90 wt. % elemental sulfur) [36], for example, has been thoroughly studied for its thermal, thermo-morphological, and mechanical properties and has been subjected to a range of ASTM and ISO tests (summarized in Table 1) [37]. These tests include simulated long-term durability to abrasion (ASTM C1353) that indicates higher durability than that of marble [38–43].

Table 1. Summary of properties of SunBG$_{90}$ with comparison to marble. Details on ASTM and ISO methodologies are provided in reference [37].

Test/Metric	Test Name/Number	Value of Metric	
		SunBG$_{90}$	**Marble**
Compressive strength	Compressive strength	35.9 MPa	12.45 MPa
Flexural strength	Flexural strength	7.7 MPa	3.4 MPa
Water absorption	ASTM C140	0.83%	0.12%
Density	ASTM C140	106.5 lb./ft^3	164.8 lb./ft^3
Abrasion resistance (I_w)	ASTM C1353	16 (unitless)	10 (unitless)
Thermal conductivity	ISO 8302	0.126 W/(m·K)	2.95 W/(m·K)
Moh's Hardness	Moh's hardness test	2.5	3

All of the reported tests on triglyceride-sulfur HSMs indicate that chemistry for successful strength development occurs over the first four days after molding at room temperature [36,44,45], by which time it has over twice the 17 MPa compressive strength required for use in residential building foundations (Figure 1) [46].

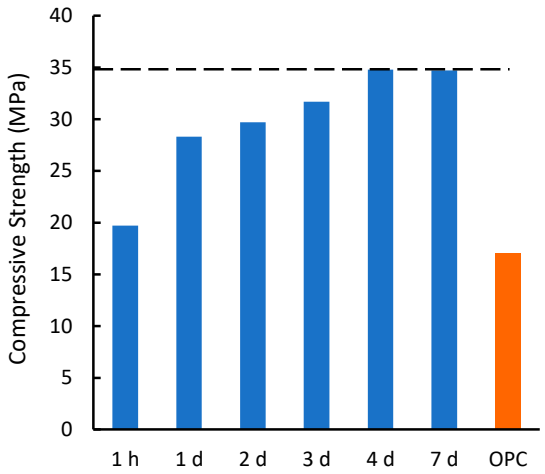

Figure 1. A plot of the changes in the compressive strength of SunBG$_{90}$ from 1 h to 7 d after casting cylinders reveals little change in compressive strength after the fourth day of setting [36]. The minimum compressive strength required of OPC for use in building foundations (17 MPa, American Concrete Institute 332.1R-06) is shown for comparison. The dotted line reflects the leveling-off of strength between 4 and 7 d.

It remains unknown how exposure to variable thermal or chemical challenges during the property-development stage of $SunBG_{90}$ might influence its strength and morphology compared to standard strength development in air at room temperature. In the current report, we allowed cylinders of $SunBG_{90}$ to stand for four days under the influence of thermal and chemical stresses to assess their influence on the strength development and thermo-morphological properties. The stresses explored were lower temperature (−25 °C), higher temperature (40 °C), and submersion in various liquids, including hydrophilic solvent (deionized water), oleophilic solvent (hexanes), high ionic strength solution (saturated NaCl(*aq*)), strongly alkaline solution (0.1 *M* NaOH(*aq*)), and a strongly acidic solution (0.1 *M* H_2SO_4).

2. Materials and Methods

2.1. Instrumentation and Calculations

DSC data were acquired (Mettler Toledo DSC 3 STARe System, Mettler Toledo, Columbus, OH, USA) over the range −60 to 140 °C with a heating rate of 10 °C·min^{-1} under a flow of N_2 (200 mL·min^{-1}). Each DSC measurement was carried out over three heat–cool cycles.

Compressional analysis was performed on a Mark-10 ES30 (Mark-10 Corporation Copiague, NY, USA) test stand equipped with an M3-200 force gauge (1 kN maximum force with ±1 N resolution) with an applied force rate of 3–4 N·s^{-1}. Compression cylinders were cast from silicone resin molds (Smooth-On Oomoo® 25 tin-cure, Oomoo Corp., Richmond, BC, Canada) with diameters of approximately 6 mm and heights of approximately 10 mm. Samples were manually sanded to ensure uniform dimensions and measured with a digital caliper with ±0.01 mm resolution. Compressional analysis was performed in triplicate and the results were averaged.

For percent crystallinity calculations, T_m, ΔH_m, and ΔH_{cc}, the data were taken from the third heat/cool cycle. Melting enthalpies and cold crystallization enthalpies were calculated using DSC data. The reduction in the percent crystallinity of the composite $SunBG_{90}$ with respect to sulfur was calculated using the following equation:

$$\Delta\chi_c = 1 - \left\{ \frac{\Delta H_{m(SunBG_{90})} - \Delta H_{cc(SunBG_{90})}}{\Delta H_{m(S)} - \Delta H_{cc(S)}} \right\} * 100\%$$

$\Delta\chi_c$—Change in percentage crystallinity with respect to sulfur
$\Delta H_{m(CFSx)}$—Melting enthalpy of composite materials ($SunBG_{90}$)
$\Delta H_{cc(CFSx)}$—Cold crystallization enthalpy of composite materials
$\Delta H_{m(S)}$—Melting enthalpy of sulfur
$\Delta H_{cc(S)}$—Cold crystallization enthalpy of sulfur

2.2. Synthesis and Exposure of Samples

The synthesis of $SunBG_{90}$ followed the reported procedure [36]. CAUTION: heating elemental sulfur with organics can result in the formation of H_2S gas. H_2S is toxic, foul-smelling, and corrosive. Although any mass loss attributable to gas generation was not observed, the temperature must be carefully controlled to prevent thermal spikes, contributing to the potential for H_2S evolution. Rapid stirring, shortened heating times, and very slow addition of reagents can help prevent unforeseen temperature spikes.

The samples labeled room temperature (RT) in the text were allowed to stand at room temperature in the dark under ambient air for four days prior to DSC and compressional strength testing reported herein.

Cylinders with diameters of approximately 6 mm and heights of approximately 10 mm, appropriate for compressive strength measurements, were prepared by melting the composite at 160 °C, then slowly and carefully pouring it into molds and allowing the material to solidify. The samples were sanded to remove flack and measured with a digital caliper with ±0.01 mm resolution. For each condition, the samples were prepared as follows:

Room Temperature (RT): The samples were allowed to stand in a dark environment for 4 d in the dark under ambient air at room temperature (22–24 °C).

Low Temperature (−25 °C): The samples were allowed to stand in a −25 °C freezer under air for 4 d.

High Temperature (40 °C): The samples were placed in an oven in a glass beaker and allowed to stand under air for 4 d.

Submerged Samples: The remaining samples were placed in a 5 mL glass vial, followed by the addition of 2 mL of the solution of interest: saturated NaCl(*aq*), 0.1 M NaOH(*aq*), 0.1 M H_2SO_4(*aq*), deionized water, or hexanes.

3. Results and Discussion

3.1. Design and Rationale

OPC has an excellent record of durability and performance but exposure to specific chemical environments can degrade its strength. At sub-freezing temperatures, for example, the properties of OPC are subject to significant detriment because water within the cement matrix freezes, leading to volumetric expansion that creates internal stresses [47,48]. This phenomenon increases susceptibility to frost damage and freeze–thaw cycles, causing cracking and spalling, even of set concrete, effects that are accentuated when cement is cast at sub-optimal temperatures, consequently compromising the cement's mechanical integrity. Conversely, at elevated temperatures (≥40 °C), OPC hydration accelerates and water evaporation during curing at higher temperatures can be problematic for installers, requiring the re-application of water to finished surfaces to prevent differential shrinkage stresses that lead to spontaneous cracking, ultimately impacting the mechanical resistance and overall durability [49].

Even in the absence of thermal stresses, exposure of OPC to water contributes to the deterioration of strength over time due to leaching, erosion, and other physical and chemical factors and standard OPC formulations cannot be cast and set where immediate submersion is necessitated. Prolonged exposure of set cement can also facilitate disparate reactions such as carbonation [50] and alkali–aggregate reactions [51], both of which are detrimental to the structural integrity of the cement. Prior to this study, it was not known how temperature could influence ultimate strength development in HSMs.

When OPC is submerged in high ionic strength aqueous solutions containing specific ions, notably chloride ions in a saturated aqueous solution of sodium chloride (NaCl), additional specific chemical degradation mechanisms become important. Chloride ions penetrate the porous cement structure, where the ions can react with calcium hydroxide and soluble silicate in the cement, forming Friedel's Salt [52] and increasing the porosity of the concrete [53,54]. In cements that have not reached full strength development or dried, chloride ion mobility is rapid, so installing fresh-set OPC in salt water applications is not recommended, requiring such installations to stand for 28 days or more before placement in many cases. Before this study, it was unknown how the submersion of freshly poured HSMs in water would influence ultimate strength development.

The pH of aqueous environments where OPC is used can also influence strength and operational lifetime. Although OPC mixtures with water are alkaline, low pH solutions, such as aqueous sulfuric acid (H_2SO_4) used in a wide range of industrial settings, significantly degrade the properties of OPC at all stages, even after it is fully set [55]. A tile of fully-cured OPC placed in even a dilute aqueous solution of H_2SO_4 loses form and chemically decomposes within hours [56]. Before this study, it was known that HSMs that had already developed to full strength were acid resistant [10,36,44,45,57,58] but it was unknown how the exposure of *freshly-poured* HSMs to high ionic strength, acidic, or alkaline solution might influence their ultimate strength development.

In addition to aqueous environments, organic solvents or other hydrophobic media can also impede the natural hydration process of concrete and the development of strength in the setting process; exposure to many organic solvents can arrest the cement hydration reaction required for setting [59]. Consequently, this may interfere with the crystalline

structure formation, leading to a decline in structural integrity and strength. Furthermore, long-term exposure to nonpolar solvents like hexanes may alter the chemical bonding between the aggregate and the cement paste and can induce microcracking. Prior to this study, it was not known how the exposure of freshly poured HSMs to hydrophobic solvents might influence their strength development.

One of the most promising HSMs under investigation as a potential OPC replacement is $SunBG_{90}$ (properties summarized in Table 1 and Figure 1) [36]. For this reason, we examined the extent to which the thermo-morphological and compressional strength characteristics of $SunBG_{90}$ were influenced when they were exposed for four days (starting immediately after cooling molten reaction mixture to room temperature) to standing at −25 °C, at 40 °C, submerged in saturated NaCl(*aq*), submerged in 0.1 M NaOH(*aq*), submerged in 0.1 M H_2SO_4(*aq*), submerged in deionized water, or submerged in hexanes. Following exposure to each stress, properties were compared to those allowed to develop strength at room temperature in ambient air.

3.2. Effects of Environmental Factors on Physical and Thermo-Morphological Properties

After $SunBG_{90}$ was exposed to the different conditions for 4 d, the dimensions of the samples and their masses were recorded for comparison to the initial values. Volumes and densities of the samples changed by <3% for all of the samples other than the sample treated with hexanes, which showed a 3.1% volume increase and concomitant density decrease due to changes in crystal morphology, as further elucidated in studies described below (dimensions and masses for pre- and post-exposed samples are provided in Table S1 of the Supplementary Materials file).

Three samples per condition were crushed into a fine powder and the thermo-morphological transitions were analyzed by differential scanning calorimetry (DSC, Figure 2, and Table 2). On the first heating cycle, all tested samples (except for hexane-exposed composites) exhibited phase transition at around 106 °C, attributable to a typical orthorhombic to monoclinic phase change and a melting point for β-sulfur (114–116 °C). In the case of hexane-exposed material, an unusual phase transition attributable to the melting of metastable γ-sulfur [60] was observed [61,62]. In integrations among sulfur allotropes, γ-sulfur is especially advantageous for use in lithium-sulfur batteries because it has a higher energy storage density than allotropes that are typically stable at standard temperature and pressure. Observing persistent γ-sulfur at room temperature is unusual but recent reports showed that it can be stabilized within a network [61], so stabilization by the crosslinked network found in $SunBG_{90}$ has precedent. We further confirmed the presence of γ-sulfur using powder X-ray diffraction (PXRD, Figure S1 in the Supplementary Materials), which confirmed a 5% contribution of γ-sulfur to the structure. Although it is not the thermodynamically preferred allotrope of sulfur, γ-sulfur does occur naturally in rare minerals like rosickyite, wherein the formation of γ-sulfur is mediated by bacterial dissolution of gypsum [63]. Short-lived samples of γ-sulfur can be grown from nonpolar solvents like hexanes [64] but will revert to α-sulfur at room temperature. In contrast, the γ-sulfur produced by soaking $SunBG_{90}$ in hexanes for four days in this study persists for at least an additional four days after its formation (the time between the DSC scan and the PXRD analysis), providing additional evidence for its stabilization within the $SunBG_{90}$ matrix.

The third DSC heating cycle (thermograms provided in Figure S2 of the Supplementary Materials) showed glass transitions between −36 and −37 °C, diagnostic for polymeric sulfur catenates, as well as cold crystallization peaks at between 6–48 °C, a range common for HSMs with intermediate lengths of sulfur crosslinking chains (intermediate range of sulfur ranks) [65–71].

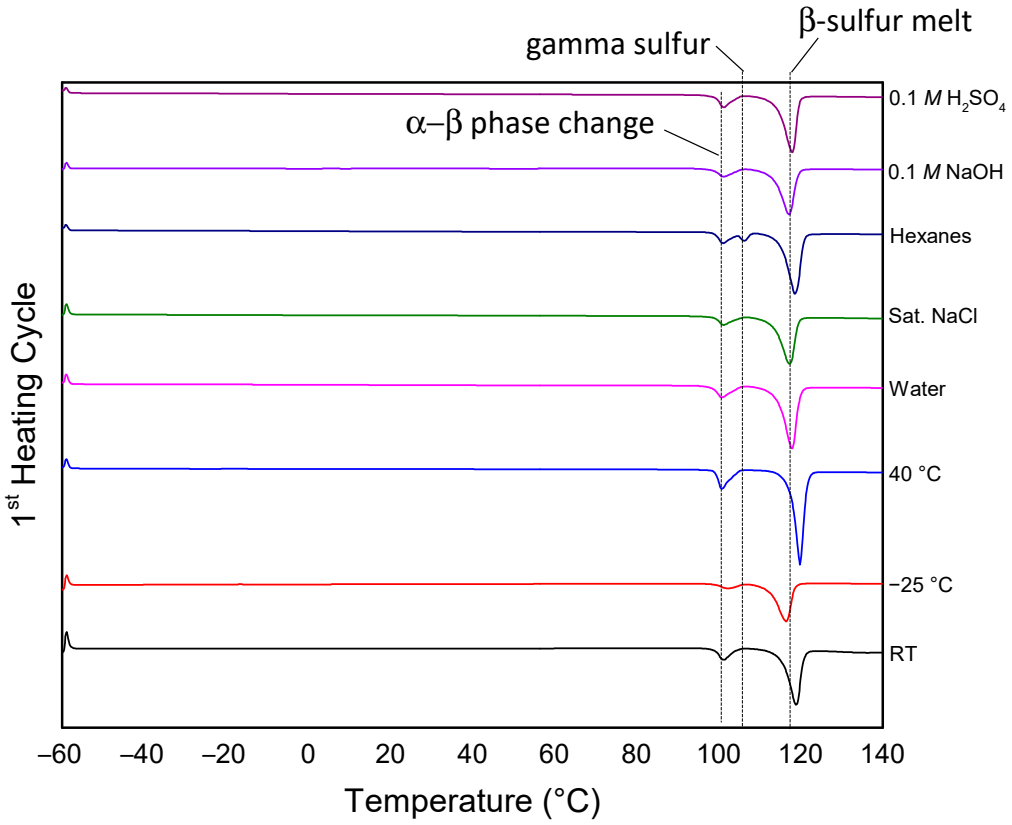

Figure 2. Differential scanning calorimetry (DSC) thermograms for $SunBG_{90}$ after 4 d exposure to various environmental factors. In these traces, endothermic is in the downward direction.

Table 2. Thermal and morphological properties of $SunBG_{90}$ exposed to different environmental conditions.

Condition	T_m [a]/°C	$T_{g,DSC}$ [b]/°C	Cold Crystallization Peaks/°C	ΔH_m J/g	ΔH_{cc} J/g	Percent Crystallinity [c]
RT	119	−36.0	NA	29.3	−2.2	30
−25 °C	118	−36.2	34	28.2	−1.5	46
40 °C	119	−36.2	NA	39.4	−1.1	10
Water	118	−36.2	NA	33.8	−1.1	22
Sat. NaCl	117	−36.2	6.1, 44	28.2	−1.5	34
Hexanes	118	−36.5	NA	34.6	−0.3	22
0.1 M NaOH	117	−36.2	47.5	28.2	−0.8	35
0.1 M H_2SO_4	117	−36.3	−0.50, 42	32.1	−0.4	27

[a] The temperature at the peak minimum of the endothermic melting from the first heating cycle. [b] Glass transition temperature from the third heating cycle. [c] The reduction in the percent crystallinity of each sample was calculated with respect to sulfur (normalized to 100%); values were taken from the first heating cycle.

The percent crystallinity of $SunBG_{90}$ relative to crystalline orthorhombic sulfur was obtained from DSC data using integrations of melting and cold crystallization enthalpies, derived from the integration of melting and cold crystallization enthalpies in the DSC data. A consistently moderate level of percent crystallinity was observed across various conditions, except extreme temperature ranges, where the values deviated from this established trend. While the percent crystallinity is also somewhat low in the hexane-exposed sample, the presence of γ-sulfur in that sample precludes a one-to-one comparison of percent crystallinity to mechanical strength predictions, as detailed below.

Powder X-ray diffraction (PXRD) was accomplished using a Rigaku SmartLab diffractometer with Cu Kα radiation (λ= 1.5406 Å) at a rate of 2°/min from 10–60° at 0.02° intervals for all thermal- and chemical-exposed samples. Polycrystalline orange crystals were removed from the hexane-exposed cylinders and analyzed via PXRD at a rate of 0.5°/min from 15–45° at 0.02° intervals to determine the presence of various sulfur polymorphs. The results obtained from PXRD analysis confirmed that the α-polymorph of sulfur predominated in all cases and that only the hexane-exposed sample showed a detectable (5%) contribution of the γ-polymorph, consistent with findings from DSC analysis (Figure 3).

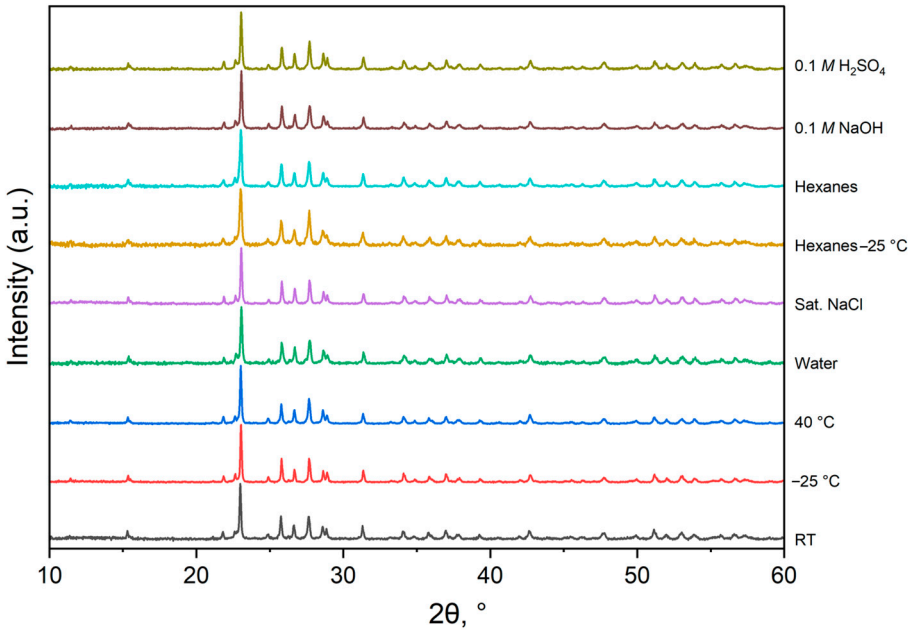

Figure 3. Powder X-ray diffraction (PXRD) results demonstrate the stability of the samples under diverse conditions.

To assess the extent to which γ-sulfur formation at hexane-exposed material was temperature-dependent, exposure of $SunBG_{90}$ to hexanes was repeated at 40 °C and −25 °C. No γ-sulfur was observed in samples exposed at 40 °C but at −25 °C a similar amount of the γ-sulfur contribution to the microstructure of $SunBG_{90}$ was observed as was observed after exposure at room temperature (modeling curves and quantification from PXRD analysis of room temperature and −25 °C experiments are provided as File S1 and S2 in the Supplementary Materials file). These data suggest that enough thermal energy is available to access exclusively thermodynamic product α-sulfur above room temperature but that a small amount of kinetically trapped metastable γ-sulfur is retained at room temperature or below at hexane-exposed surfaces.

3.3. Effects of Environmental Stresses on Compressional Strength Development

To prepare cylinders for testing, $SunBG_{90}$ composite was melted at 160 °C, slowly poured into silicon molds, and allowed to solidify by cooling over about 30 min to room temperature. Cylinders were then allowed to develop strength over four days at ambient conditions or exposed to environmental stresses (Figure 4). Unsurprisingly, most cylinders exhibited little visually discernible changes over this test period. However, cylinders exposed to hexanes displayed surface and color alterations due to the surface crystallization of various forms of sulfur (later discerned more conclusively by DSC and PXRD analysis).

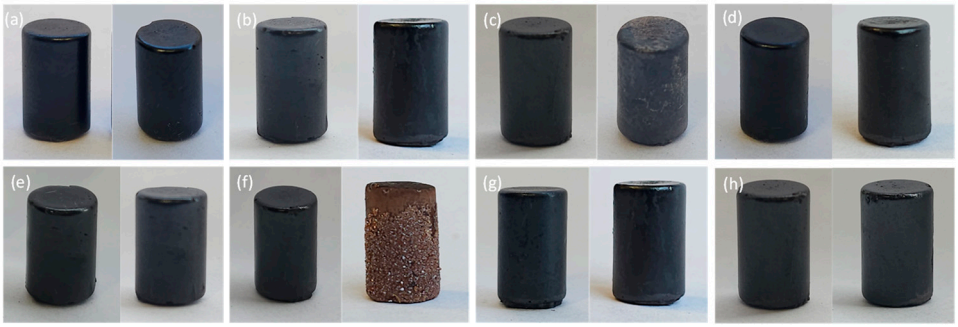

Figure 4. Each panel shows the visual appearance of compressive testing cylinders as-cast (left) and after aging for four days (right) under the various environmental conditions: (**a**) room temperature, (**b**) −25 °C, (**c**) 40 °C, (**d**) water, (**e**) sat. NaCl, (**f**) hexanes, (**g**) 0.1 M NaOH, and (**h**) 0.1 M H_2SO_4.

The compressive strength for each composite was measured in triplicate using a mechanical test stand (Figure 5; stress–strain curves are provided in Figures S3–S10 in the Supplementary Materials). These data reveal that neither low temperature nor submersion in solvents/solutions adversely affected the compressive strength of $SunBG_{90}$. A small but statistically significant increase in compressive strength was observed when $SunBG_{90}$ developed strength while submerged in aqueous solutions. This observation could be simply a result of faster initial cooling of the samples upon submersion in the samples, as no other significant morphological changes were noted under any of these conditions.

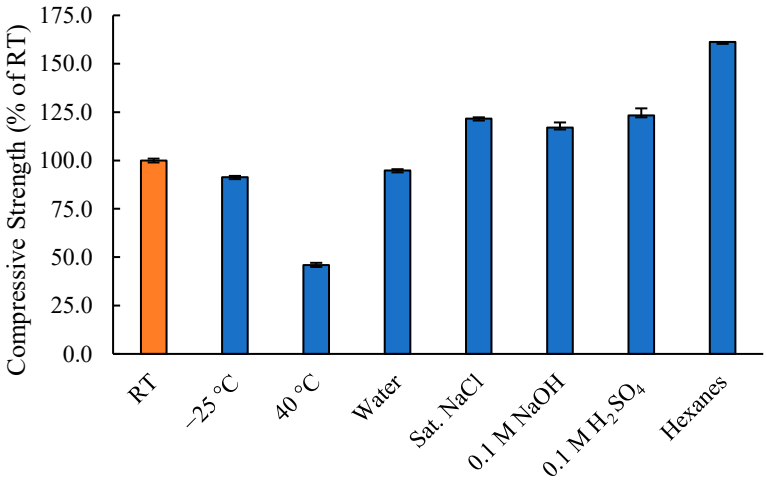

Figure 5. Compressive strength of $SunBG_{90}$ composites after 4 d exposure to various conditions compared to OPC.

Exposure to higher temperature (40 °C) during strength development was the only stress screened that had a notably deleterious effect on the compressive strength, which was reduced by almost 50% compared to when strength development occurs at room temperature (20 °C). This is perhaps unsurprising given that the sample subjected to an elevated temperature has less than half the percent crystallinity of any other samples (Table 2). The sample exposed to hexanes also has a notably lower crystallinity than all but the 40 °C-treated samples but the development of a hard crystalline "crust" on the exterior of the compressive strength test cylinder developed in hexanes and the presence of γ-sulfur within the crystal lattice both reinforce this cylinder such that the compressive strength of the hexane-developed cylinder is approximately 50% higher than samples developed at room temperature.

In Table 3, we present the quantitative compressive strength results for environmentally exposed samples of $SunBG_{90}$, along with three compositionally similar previously reported sulfur materials made using triglycerides. The compressive strengths of

$SunBG_{90}$ under various environmental exposures demonstrate its resilience and versatility. $SunBG_{90}$ exhibited a compressive strength of 35.9 MPa at room temperature, surpassing conventional mineral-based masonry products such as clay bricks (10 MPa) [72] and OPC (17 MPa). Even when subjected to extreme conditions, such as exposure to −25 °C (32.8 MPa), 40 °C (16.5 MPa), or immersion in harsh chemical environments (e.g., 0.1 M NaOH, 42 MPa; 0.1 M H_2SO_4, 44.3 MPa), $SunBG_{90}$ maintained impressive compressive strengths, outperforming existing materials in the marketplace. When exposed to hexanes, $SunBG_{90}$ achieved a remarkable compressive strength of 57.9 MPa, further highlighting its superior mechanical performance. Compared with three compositionally similar sulfur materials, CanS (90 wt. %sulfur and 10 wt. %canola oil), SunS (90 wt. %sulfur and 10 wt. %sunflower oil), and CFS_{90} (90 wt. %sulfur, 5 wt. %chicken fat, and 5 wt. %canola oil) [44], $SunBG_{90}$ consistently exhibited higher compressive strengths across all environmental exposures, emphasizing its potential as a robust and durable construction material with improved mechanical properties.

Table 3. Summary of compressive strength of SunBG90 under different environmental conditions in comparison to different HSMs and mineral-based masonry products.

Composite/Material		Compressive Strength (MPa)
$SunBG_{90}$	RT	35.9
	−25 °C	32.8
	40 °C	16.5
	Water	34.0
	Sat. NaCl	43.7
	Hexanes	42.0
	0.1 M NaOH	44.3
	0.1 M H_2SO_4	57.9
CanS		9.3
SunS		17.9
CFS_{90}		24.7
Clay bricks		10.0
OPC		17.0

4. Conclusions

This study has provided valuable insights into the influence of environmental stresses on the thermo-morphological properties and strength development of $SunBG_{90}$, a high-sulfur content material with theoretical potential to replace traditional cement. DSC analysis revealed thermo-morphological transitions and the stabilization of γ-sulfur within the $SunBG_{90}$ crosslinked matrix. The presence of γ-sulfur was further confirmed through powder XRD, establishing its 5% contribution to the material's structure [73–76]. Although strength development at higher temperatures (40 °C) significantly reduced the ultimate compressive strength of $SunBG_{90}$, the strength was either unchanged or improved when $SunBG_{90}$ cylinders were exposed to aqueous acid, aqueous base, high ionic strength solution, low temperature (−25 °C), or hexanes during strength development. These findings are an important incremental step toward the possible eventual application of sulfur polymer cement in construction and industrial contexts, as they demonstrate the material's potential to withstand various environmental challenges.

Furthermore, the study contributes to the ongoing effort to develop sustainable alternatives to traditional cement, addressing the ecological concerns associated with its production. Future research is underway to investigate how comonomer structure and ratio can improve the resistance of HSMs to environmental stresses and accelerate strength

development. These efforts will be significant for accomplishing the broader goals of advancing eco-friendly construction materials and reducing the ecological impacts of the built environment.

Supplementary Materials: The following supporting information can be downloaded at: https://www.mdpi.com/article/10.3390/macromol4020013/s1, Figure S1. Powder-XRD traces for $SunBG_{90}$ structure, confirming the contribution of γ-sulfur after exposure to hexanes.; Figure S2. Differential scanning calorimetry (DSC) traces for $SunBG_{90}$ showing the third heating cycle after exposure to different environmental conditions.; Figure S3. Stress-strain plots for measurements of the compressive strength of $SunBG_{90}$ after 4d at room temperature.; Figure S4. Stress-strain plots for measurements of the compressive strength of $SunBG_{90}$ after 4d exposure at –25 °C.; Figure S5. Stress-strain plots for measurements of the compressive strength of $SunBG_{90}$ after 4d exposure at 40 °C.; Figure S6. Stress-strain plots for measurements of the compressive strength of $SunBG_{90}$ after 4d exposure to water.; Figure S7. Stress-strain plots for measurements of the compressive strength of $SunBG_{90}$ after 4d exposure to saturated NaCl.; Figure S8. Stress-strain plots for measurements of the compressive strength of $SunBG_{90}$ after 4d exposure to 0.1 M NaOH.; Figure S9. Stress-strain plots for measurements of the compressive strength of $SunBG_{90}$ after 4d exposure to 0.1 M H_2SO_4.; Figure S10. Stress-strain plots for measurements of the compressive strength of $SunBG_{90}$ after 4d exposure to hexanes.; Table S1. Dimensional analysis and masses of samples before and after exposure to environmental factors. Samples were cylindrical in shape, so that L1 and L2 represent lengths (heights) of the cylinders measured at two positions with calipers, and D1–4 are diameters cross-section measured at four positions using calipers. The height and diameter used for volume calculations are the average of the individual caliper measurements for a given cylinder.; Supporting Information File S1: Modelling of gamma-sulfur contribution to microstructure after exposure to hexanes at room temperature; Supporting Information File S2: Modelling of gamma-sulfur contribution to microstructure after exposure to hexanes at –25 °C.

Author Contributions: Conceptualization, R.C.S.; methodology, R.C.S.; formal analysis, P.Y.S.-O.; investigation, P.Y.S.-O.; resources, R.C.S. and A.D.S.; data curation, P.Y.S.-O.; writing—original draft preparation, P.Y.S.-O.; writing—review and editing, all authors; supervision, R.C.S. and A.D.S.; funding acquisition, R.C.S. and A.D.S. All authors have read and agreed to the published version of the manuscript.

Funding: This research was funded by The National Science Foundation grant number CHE-2203669 to R.C.S. and a seed grant from the Animal Coproducts Research and Education Center to R.C.S. and A.D.S.

Data Availability Statement: The original contributions presented in the study are included in the article/Supplementary Material, further inquiries can be directed to the corresponding authors.

Conflicts of Interest: The authors declare no conflicts of interest.

References

1. Gutarowska, B.; Piotrowska, M.; Kozirog, A.; Berlowska, J.; Dziugan, P.; Kotynia, R.; Bielinski, D.; Anyszka, R.; Wreczycki, J. New Sulfur Organic Polymer-Concrete Composites Containing Waste Materials: Mechanical Characteristics and Resistance to Biocorrosion. *Materials* **2019**, *12*, 2602. [CrossRef] [PubMed]
2. Lewandowski, M.; Kotynia, R. Assessment of sulfur concrete properties for use in civil engineering. *MATEC Web Conf.* **2018**, *219*, 3006. [CrossRef]
3. Gwon, S.; Jeong, Y.; Oh, J.E.; Shin, M. Sustainable sulfur composites with enhanced strength and lightweightness using waste rubber and fly ash. *Constr. Build. Mater.* **2017**, *135*, 650–664. [CrossRef]
4. Smith, A.D.; Smith, R.C.; Tennyson, A.G. Polymer cements by copolymerization of waste sulfur, oleic acid, and pozzolan cements. *Sust. Chem. Pharm.* **2020**, *16*, 100249. [CrossRef]
5. Scrivener, K.L.; John, V.M.; Gartner, E.M. Eco-efficient cements: Potential economically viable solutions for a low-CO_2 cement-based materials industry. *Cem. Concr. Res.* **2018**, *114*, 2–26. [CrossRef]
6. Furtos, G.; Molnar, L.; Silaghi-Dumitrescu, L.; Pascuta, P.; Korniejenko, K. Mechanical and thermal properties of wood fiber reinforced geopolymer composites. *J. Nat. Fibers* **2022**, *19*, 6676–6691. [CrossRef]
7. Furtos, G.; Silaghi-Dumitrescu, L.; Pascuta, P.; Sarosi, C.; Korniejenko, K. Mechanical Properties of Wood Fiber Reinforced Geopolymer Composites with Sand Addition. *J. Nat. Fibers* **2021**, *18*, 285–296. [CrossRef]
8. Weil, E.D. Recent industrial organosulfur chemistry. *Phosphorus Sulfur Silicon Relat. Elem.* **1991**, *59*, 325–340. [CrossRef]

9. Thiounn, T.; Karunarathna, M.S.; Slann, L.M.; Lauer, M.K.; Smith, R.C. Sequential Crosslinking for Mechanical Property Development in High Sulfur Content Composites. *J. Poly. Sci.* **2020**, *58*, 2943–2950. [CrossRef]
10. Thiounn, T.; Tennyson, A.G.; Smith, R.C. Durable, acid-resistant copolymers from industrial by-product sulfur and microbially-produced tyrosine. *RSC Adv.* **2019**, *9*, 31460–31465. [CrossRef]
11. Gregor, R.; Hackl, A. A new approach to sulfur concrete. *Adv. Chem. Ser.* **1978**, *165*, 54–78.
12. Shrive, N.G.; Gillott, J.E.; Jordaan, I.J.; Loov, R.E. The potential and properties of sulfur concretes. *ACS Symp. Ser.* **1982**, *183*, 137–154. [CrossRef]
13. Okumura, H.A. Early sulfur concrete installations. *Concr. Int.* **1998**, *20*, 72–75.
14. Davis, A.E.; Sayer, K.B.; Jenkins, C.L. A comparison of adhesive polysulfides initiated by garlic essential oil and elemental sulfur to create recyclable adhesives. *Polym. Chem.* **2022**, *13*, 4634–4640. [CrossRef]
15. Eder, M.L.; Call, C.B.; Jenkins, C.L. Utilizing Reclaimed Petroleum Waste to Synthesize Water-Soluble Polysulfides for Selective Heavy Metal Binding and Detection. *ACS Appl. Polym. Mater.* **2022**, *4*, 1110–1116. [CrossRef]
16. Eder, M.L.; Jenkins, C. Inverse vulcanization of sulfur and charged monomers to enhance solubility and create inexpensive metal binding materials. *Abstr. Pap. Am. Chem. Soc.* **2019**, *257*, POLY-0336.
17. Herrera, C.; Ysinga, K.J.; Jenkins, C.L. Polysulfides Synthesized from Renewable Garlic Components and Repurposed Sulfur Form Environmentally Friendly Adhesives. *ACS Appl. Mater. Interfaces* **2019**, *11*, 35312–35318. [CrossRef]
18. Orme, K.; Fistrovich, A.H.; Jenkins, C.L. Tailoring Polysulfide Properties through Variations of Inverse Vulcanization. *Macromolecules* **2020**, *53*, 9353–9361. [CrossRef]
19. Westerman, C.R.; Jenkins, C.L. Dynamic Sulfur Bonds Initiate Polymerization of Vinyl and Allyl Ethers at Mild Temperatures. *Macromolecules* **2018**, *51*, 7233–7238. [CrossRef]
20. Duarte, M.E.; Huber, B.; Theato, P.; Mutlu, H. The unrevealed potential of elemental sulfur for the synthesis of high sulfur content bio-based aliphatic polyesters. *Polym. Chem.* **2020**, *11*, 241–248. [CrossRef]
21. Nguyen, D.T.; Hoefling, A.; Yee, M.; Nguyen, G.T.H.; Theato, P.; Lee, Y.J.; Song, S.-W. Enabling High-Rate and Safe Lithium Ion-Sulfur Batteries by Effective Combination of Sulfur-Copolymer Cathode and Hard-Carbon Anode. *ChemSusChem* **2019**, *12*, 480–486. [CrossRef]
22. Mutlu, H.; Theato, P.; Ceper Ezgi, B.; Ozmen Mehmet, M.; Li, X.; Yang, J.; Dong, W.; Theato, P.; Yang, J. Sulfur Chemistry in Polymer and Materials Science. *Macromol. Rapid Commun.* **2019**, *40*, e1800650. [CrossRef]
23. Dale, J.J.; Stanley, J.; Dop, R.A.; Chronowska-Bojczuk, G.; Fielding, A.J.; Neill, D.R.; Hasell, T. Exploring Inverse Vulcanisation Mechanisms from the Perspective of Dark Sulfur. *Eur. Polym. J.* **2023**, *195*, 112198. [CrossRef]
24. Jia, J.; Liu, J.; Wang, Z.-Q.; Liu, T.; Yan, P.; Gong, X.-Q.; Zhao, C.; Chen, L.; Miao, C.; Zhao, W.; et al. Photoinduced inverse vulcanization. *Nat. Chem.* **2022**, *14*, 1249–1257. [CrossRef]
25. Dale, J.J.; Petcher, S.; Hasell, T. Dark Sulfur: Quantifying Unpolymerized Sulfur in Inverse Vulcanized Polymers. *ACS Appl. Polym. Mater.* **2022**, *4*, 3169–3173. [CrossRef]
26. Dodd, L.J.; Omar, O.; Wu, X.; Hasell, T. Investigating the Role and Scope of Catalysts in Inverse Vulcanization. *ACS Catal.* **2021**, *11*, 4441–4455. [CrossRef]
27. Tonkin, S.J.; Gibson, C.T.; Campbell, J.A.; Lewis, D.A.; Karton, A.; Hasell, T.; Chalker, J.M. Chemically induced repair, adhesion, and recycling of polymers made by inverse vulcanization. *Chem. Sci.* **2020**, *11*, 5537–5546. [CrossRef] [PubMed]
28. Tikoalu, A.D.; Lundquist, N.A.; Chalker, J.M. Mercury Sorbents Made By Inverse Vulcanization of Sustainable Triglycerides: The Plant Oil Structure Influences the Rate of Mercury Removal from Water. *Adv. Sustain. Syst.* **2020**, *4*, 1900111. [CrossRef]
29. Mann, M.; Kruger, J.E.; Andari, F.; McErlean, J.; Gascooke, J.R.; Smith, J.A.; Worthington, M.J.H.; McKinley, C.C.C.; Campbell, J.A.; Lewis, D.A.; et al. Sulfur polymer composites as controlled-release fertilizers. *Org. Biomol. Chem.* **2019**, *17*, 1929–1936. [CrossRef]
30. Worthington, M.J.H.; Kucera, R.L.; Chalker, J.M. Green chemistry and polymers made from sulfur. *Green Chem.* **2017**, *19*, 2748–2761. [CrossRef]
31. Bao, J.; Martin, K.P.; Cho, E.; Kang, K.-S.; Glass, R.S.; Coropceanu, V.; Bredas, J.-L.; Parker, W.O.N., Jr.; Njardarson, J.T.; Pyun, J. On the Mechanism of the Inverse Vulcanization of Elemental Sulfur: Structural Characterization of Poly(sulfur-random-(1,3-diisopropenylbenzene)). *J. Am. Chem. Soc.* **2023**, *145*, 12386–12397. [CrossRef] [PubMed]
32. Lee, T.; Dirlam, P.T.; Njardarson, J.T.; Glass, R.S.; Pyun, J. Polymerizations with Elemental Sulfur: From Petroleum Refining to Polymeric Materials. *J. Am. Chem. Soc.* **2022**, *144*, 5–22. [CrossRef]
33. Zhang, Y.; Glass, R.S.; Char, K.; Pyun, J. Recent advances in the polymerization of elemental sulphur, inverse vulcanization and methods to obtain functional Chalcogenide Hybrid Inorganic/Organic Polymers (CHIPs). *Polym. Chem.* **2019**, *10*, 4078–4105. [CrossRef]
34. Kolet, M.; Zerbib, D.; Nakonechny, F.; Nisnevitch, M. Production of Biodiesel from Brown Grease. *Catalysts* **2020**, *10*, 1189. [CrossRef]
35. Sim, Y.-L.; Meyappan, N.; Yen, N.S.; Kamala a/p Subramaniam, S.; Khoo, C.H.; Cheah, W.L.; St. Hilaire, D.; Pinnock, T.; Bacolod, B.; Cai, Z.B.; et al. Chemical reactions in the pyrolysis of brown grease. *Fuel* **2017**, *207*, 274–282. [CrossRef]
36. Lopez, C.V.; Smith, A.D.; Smith, R.C. High strength composites from low-value animal coproducts and industrial waste sulfur. *RSC Adv.* **2022**, *12*, 1535–1542. [CrossRef] [PubMed]
37. Sauceda-Olono, P.Y.; Borbon-Almada, A.C.; Gaxiola, M.; Smith, A.D.; Tennyson, A.G.; Smith, R.C. Thermal and Mechanical Properties of Recyclable Composites Prepared from Bio-Olefins and Industrial Waste. *J. Compos. Sci.* **2023**, *7*, 248. [CrossRef]

38. Ruedrich, J.; Knell, C.; Enseleit, J.; Rieffel, Y.; Siegesmund, S. Stability assessment of marble statuaries of the Schlossbrücke (Berlin, Germany) based on rock strength measurements and ultrasonic wave velocities. *Environ. Earth Sci.* **2013**, *69*, 1451–1469. [CrossRef]
39. Ozcelik, Y.; Ozguven, A. Water absorption and drying features of different natural building stones. *Constr. Build. Mater.* **2014**, *63*, 257–270. [CrossRef]
40. Medvedev, V.Y.; Stepanov, P. Density characteristics of ancient rocks of the western tien-shan. *Int. Geol. Rev.* **1962**, *4*, 67–78. [CrossRef]
41. Choudhary, R. An Experimental Investigation to Evaluate Abrasion Wear Characteristics and Study the Effect of Micro Cracks on the Mechanical Properties of Various Marbles Types of Rajasthan Region. Doctoral Dissertation, MNIT, Jaipur, India, 2015.
42. Broz, M.E.; Cook, R.F.; Whitney, D.L. Microhardness, toughness, and modulus of Mohs scale minerals. *Am. Mineral.* **2006**, *91*, 135–142. [CrossRef]
43. Marble Institute of America. Report 2016-VIII. In *Stone Testing*; Marble Institute of America: Oberlin, OH, USA, 2016.
44. Lopez, C.V.; Smith, A.D.; Smith, R.C. Evaluation of Animal Fats and Vegetable Oils as Comonomers in Polymer Composite Synthesis: Effects of Plant/Animal Sources and Comonomer Composition on Composite Properties. *Macromol. Chem. Phys.* **2023**, *9*, 2300233. [CrossRef]
45. Lopez, C.V.; Karunarathna, M.S.; Lauer, M.K.; Maladeniya, C.P.; Thiounn, T.; Ackley, E.D.; Smith, R.C. High Strength, Acid-Resistant Composites from Canola, Sunflower, or Linseed Oils: Influence of Triglyceride Unsaturation on Material Properties. *J. Poly. Sci.* **2020**, *58*, 2259–2266. [CrossRef]
46. ACI Committee 332. *Guide to Residential Concrete Construction*; ACI 332.1R-06, American Concrete Institute: Farmington Hills, MI, USA, 2006.
47. Liu, L.; Shen, D.; Chen, H.; Sun, W.; Qian, Z.; Zhao, H.; Jiang, J. Analysis of damage development in cement paste due to ice nucleation at different temperatures. *Cem. Concr. Compos.* **2014**, *53*, 1–9. [CrossRef]
48. Wu, M.; Fridh, K.; Johannesson, B.; Geiker, M. Influence of frost damage and sample preconditioning on the porosity characterization of cement based materials using low temperature calorimetry. *Thermochim. Acta* **2015**, *607*, 30–38. [CrossRef]
49. Fu, Y.-F.; Wong, Y.-L.; Poon, C.-S.; Tang, C.-A.; Lin, P. Experimental study of micro/macro crack development and stress–strain relations of cement-based composite materials at elevated temperatures. *Cem. Concr. Res.* **2004**, *34*, 789–797. [CrossRef]
50. Fabbri, A.; Corvisier, J.; Schubnel, A.; Brunet, F.; Goffé, B.; Rimmele, G.; Barlet-Gouédard, V. Effect of carbonation on the hydro-mechanical properties of Portland cements. *Cem. Concr. Res.* **2009**, *39*, 1156–1163. [CrossRef]
51. Sanchez, L. Contribution to the Assessment of Damage in Aging Concrete Infrastructures Affected by Alkali-Aggregate Reaction. Doctoral Dissertation, Université Laval, Québec, QC, Canada, 2014.
52. Qiao, C.; Suraneni, P.; Weiss, J. Damage in cement pastes exposed to NaCl solutions. *Constr. Build. Mater.* **2018**, *171*, 120–127. [CrossRef]
53. Qiao, C.; Suraneni, P.; Tsui Chang, M.; Weiss, J. Damage in cement pastes exposed to $MgCl_2$ solutions. *Mater. Struct.* **2018**, *51*, 1–15. [CrossRef]
54. Hosseinzadeh, N.; Montanari, L.; Qiao, C.; Suraneni, P. Damage in cement pastes and mortars exposed to $CaCl_2$ and low-temperature cycles. *Mater. Struct.* **2022**, *55*, 105. [CrossRef]
55. Zivica, V.r.; Bajza, A. Acidic attack of cement based materials—A review: Part 1. Principle of acidic attack. *Constr. Build. Mater.* **2001**, *15*, 331–340. [CrossRef]
56. Lauer, M.K.; Estrada-Mendoza, T.A.; McMillen, C.D.; Chumanov, G.; Tennyson, A.G.; Smith, R.C. Durable Cellulose-Sulfur Composites Derived from Agricultural and Petrochemical Waste. *Adv. Sustain. Syst.* **2019**, *3*, 1900062. [CrossRef]
57. Tisdale, K.A.; Maladeniya, C.P.; Lopez, C.V.; Tennyson, A.G.; Smith, R.C. Sustainable Composites from Waste Sulfur, Terpenoids, and Pozzolan Cements. *J. Compos. Sci.* **2023**, *7*, 35. [CrossRef]
58. Graham, M.J.; Lopez, C.V.; Maladeniya, C.P.; Tennyson, A.G.; Smith, R.C. Influence of pozzolans on plant oil-sulfur polymer cements: More sustainable and chemically-resistant alternatives to Portland cement. *J. Appl. Polym. Sci.* **2023**, *140*, e53684. [CrossRef]
59. Zhang, J.; Scherer, G.W. Comparison of methods for arresting hydration of cement. *Cem. Concr. Res.* **2011**, *41*, 1024–1036. [CrossRef]
60. Muthmann, W. XXIV. Untersuchungen über den Schwefel und das Selen. *Z. Für Krist. Cryst. Mater.* **1890**, *17*, 336–367. [CrossRef]
61. Pai, R.; Singh, A.; Tang, M.H.; Kalra, V. Stabilization of gamma sulfur at room temperature to enable the use of carbonate electrolyte in Li-S batteries. *Commun. Chem.* **2022**, *5*, 17. [CrossRef] [PubMed]
62. Kang, H.; Park, M.J. Thirty-minute synthesis of hierarchically ordered sulfur particles enables high-energy, flexible lithium-sulfur batteries. *Nano Energy* **2021**, *89*, 106459. [CrossRef]
63. Douglas, S.; Yang, H. Mineral biosignatures in evaporites: Presence of rosickyite in an endoevaporitic microbial community from Death Valley, California. *Geology* **2002**, *30*, 1075–1078. [CrossRef]
64. Greenwood, N.N.; Earnshaw, A. *Chemistry of the Elements*; Elsevier: Amsterdam, The Netherlands, 2012.
65. Khawaja, S.Z.; Kumar, S.V.; Jena, K.K.; Alhassan, S.M. Flexible sulfur film from inverse vulcanization technique. *Mater. Lett.* **2017**, *203*, 58–61. [CrossRef]
66. Lian, Q.; Li, Y.; Li, K.; Cheng, J.; Zhang, J. Insights into the vulcanization mechanism through a simple and facile approach to the sulfur cleavage behavior. *Macromolecules* **2017**, *50*, 803–810. [CrossRef]

67. Meyer, B. Solid allotropes of sulfur. *Chem. Rev.* **1964**, *64*, 429–451. [CrossRef]
68. Meyer, B. Elemental sulfur. *Chem. Rev.* **1976**, *76*, 367–388. [CrossRef]
69. Shankarayya Wadi, V.K.; Jena, K.K.; Khawaja, S.Z.; Yannakopoulou, K.; Fardis, M.; Mitrikas, G.; Karagianni, M.; Papavassiliou, G.; Alhassan, S.M. NMR and EPR structural analysis and stability study of inverse vulcanized sulfur copolymers. *ACS Omega* **2018**, *3*, 3330–3339. [CrossRef] [PubMed]
70. Tobolsky, A.; MacKnight, W.; Beevers, R.; Gupta, V. The glass transition temperature of polymeric sulphur. *Polymer* **1963**, *4*, 423–427. [CrossRef]
71. Tobolsky, A.V. Polymeric sulfur and related polymers. In *Proceedings of the Journal of Polymer Science Part C: Polymer Symposia*; Wiley Subscription Services, Inc.: Hoboken, NJ, USA, 1966; pp. 71–78.
72. Dawood, A.O.; Mussa, F.I.; Al Khazraji, H.; Abd Ulsada, H.A.; Yasser, M.M. Investigation of compressive strength of straw reinforced unfired clay bricks for sustainable building construction. *Civ. Environ. Eng.* **2021**, *17*, 150–163. [CrossRef]
73. Coppens, P.; Yang, Y.; Blessing, R.; Copper, W.; Larsen, F. The experimental charge distribution in sulfur containing molecules. Analysis of cyclic octasulfur at 300 and 100 K. *J. Am. Chem. Soc.* **1977**, *99*, 760–766. [CrossRef]
74. Gallacher, A.; Pinkerton, A. A redetermination of monclinic γ-sulfur. *Acta Crystallogr. Sect. C Cryst. Struct. Commun.* **1993**, *49*, 125–126. [CrossRef]
75. Rettig, S.; Trotter, J. Refinement of the structure of orthorhombic sulfur, α-S8. *Acta Crystallogr. Sect. C Cryst. Struct. Commun.* **1987**, *43*, 2260–2262. [CrossRef]
76. Templeton, L.K.; Templeton, D.H.; Zalkin, A. Crystal structure of monoclinic sulfur. *Inorg. Chem.* **1976**, *15*, 1999–2001. [CrossRef]